International Journal of Computing and Digital Systems
ISSN (2210-142X)
Int. J. Com. Dig. Sys. 9, No.1 (Jan-2020)
http://dx.doi.org/10.12785/ijcds/090103

Computer-aided Lymph Node Detection using Pelvic Magnetic Resonance Imaging

Nesrine Bnouni [1,2], Islem Rekik [2,3], Mohamed Salah Rhim[4] and Najoua Essoukri Ben Amara[1]

[1]*Université de Sousse, École Nationale d'Ingénieurs de Sousse, LATIS-Laboratory of Advanced Technology and Intelligent Systems, Sousse 4023, Tunisia;*
[2]*BASIRA lab, Faculty of Computer and Informatics Engineering, Istanbul Technical University, Turkey*
[3]*School of Science and Engineering, University of Dundee, Dundee DD1HN, U.K*
[4]*Department of Gynecology Obstetrics, Faculty of Medicine of Monastir, Tunisia*

Received 31 May 2019, Revised 30 Sep. 2019, Accepted 03 Nov. 2019, Published 01 Jan. 2020

Abstract: Pelvic Lymph Nodes (PLNs) segmentation and classification are fundamental tools in the medical image analysis of pelvic gynecological cancer such as endometrial and cervical cancer. Often used by the radiologist, PLN classification requires detailed knowledge of the morphological features of PLNs, derived from size, shape, contour and heterogeneous appearance. Accurate PLN segmentation is an essential step in PLN classification. In order to supply the best assessment of a nodal status, semi-automatic and automatic PLN segmentation and classification methods are highly desired as they can strongly capture the wide variability in morphological features and reduce classification errors due to the inter and intra-observer variability, while avoiding the time-consuming for manual delineation of PLN boundary. Nevertheless, semi-automatic segmentation methods require the clinician intervention to select the initial seed point. However, typical semi-automatic PLN segmentation methods might fail due to (1) the intensity inhomogeneity, noise and low contrast in medical images, and (2) the position of the starting point. Thus, the performance of these methods can be enhanced by using a preprocessing-based iterative segmentation approach. Currently, Magnetic Resonance Imaging (MRI) is the most common imaging modality used for staging endometrial and cervical cancer, evaluation of PLN involvement and selection of therapeutic strategy. PLN detection using classic features can be challenging due to the similarity between normal and abnormal PLNs structures. In pelvic cancer and metastatic PLN, Diffusion Weighted (DW)-MRI exhibits brighter areas indicating tumor and metastatic PLN. This paper combines anatomic T2-Weighted (T2-w) imaging with DW imaging. Specifically, we propose a computer-aided pelvic framework, which leverages (1) an ensemble preprocessing method to improve PLN segmentation, (2) the iterative correction of the position of the initial point by executing the segmentation algorithm several times in succession, (3) the fusion of structural and diffusion MRI and, (4) the extraction of morphological features of segmented PLNs (axial T2-w image) as well as intensity feature derived from the fused image for the final classification of PLNs as suspect or non-suspect. Research in the field of PLN detection is important as it can help doctors to better detect cervical and endometrial cancer and decide the appropriate treatment. To the best of our knowledge, this is the first work to segment and classify PLN. Our preprocessing-based iterative segmentation approach significantly ($p<0.05$) improved comparison segmentation methods, with a segmentation accuracy boosted from 61.37% for the conventional region-growing algorithm to 66.53% for the proposed method. Furthermore, we obtained an average accuracy of 78.50% for pelvic nodule classification.

Keywords: Pelvic lymph nodes, Endometrial and cervical cancer; Ensemble preprocessing boosting strategy; Iterative; segmentation; Classification; Multimodal image fusion; MRI; Normal and abnormal node detection

1. INTRODUCTION

Endometrial and cervical cancer are the mostly common gynecologic malignancies in the world. The clinical stage [1] is based on the prognostic factors like the tumor volume [2] and the nodal status. Cancer can spread to other part of the body and/or through the lymph system. Pelvic Lymph Nodes (PLNs) involvement is a very wicked prognostic factor [3]. The ganglionic status affects the patient survival and guides the choice of treatment planning. Furthermore, PLN is small oval-shape organ, in the order of a few millimeters, which is difficult to classify (suspect/ non-suspect) and confides on the radiologist's experience. Affected PLNs are typically enlarged and are evaluated by the recist criterion [4]. Indeed, the PLN size, shape, contour and heterogeneous appearance can determine its metastatic detection and give significant information about the disease and the effectiveness of the treatment. Using

E-mail address: nesrine.bnouni@gmail.com, islem.rekik@gmail.com, medsalah84@yahoo.fr, najoua.benamara@eniso.rnu.tn

automatic methods to extract these morphological features might help decrease inter and intra-observer variability and in a subsequent stage avoids a PLN dissection, which might have an impact on patient survival. Surgical lymphadenectomy is considered as the gold standard for the diagnosis of PLN metastasis, but it is routinely affected with an invasive and expensive process and an elevated risk of complications [5]. If metastatic PLNs are found at surgery, adjuvant treatment is adopted. In clinical practice, radiologists commonly have to evaluate PLNs status, which requires to segment and classify PLNs. However, finding the exact measurement and characteristic of PLNs by hand is time consuming, subjective and highly complex. Therefrom, semi-automatic and automatic PLN segmentation and classification methods are greatly needed as they can reduce segmentation and subsequently classification errors. Nevertheless, semi-automatic segmentation and automatic PLN methods might fail due to (1) the intensity inhomogeneity, poor contrast, and noise often present in medical images, and (2) the selection of the initial point that can largely influence the segmentation results. In cervix and uterus cancer, physicians typically use Magnetic Resonance Imaging (MRI) for evaluation. MRI is well-considered as the gold standard for staging and treatment planning of pelvic cancer. While axial T2-Weighted (T2-w)-MRI is classically used for the evaluation of the PLNs [6], Diffusion Weighted (DW)-MRI improves tumor delineation and detection of PLNs metastasis in pelvic cancer [7]. Specifically, DW-MRI visualizes metastatic PLNs as bright regions. To leverage the complementary sides of both anatomical T2-w and DW imaging modalities, we propose a novel approach to fuse the axial T2-w and the DW images. We segment PLNs afterwards and we combine the morphological features provided by each modality to finally classify PLNs.

Image fusion has gained more popularity in the analysis of multimodal medical images. Several fusion approaches used in medical images were analyzed in [8], such as morphological, knowledge-based, neural-network-based, wavelet-based and fuzzy-logic-based methods. Multimodal medical image fusion techniques have shown great success in the clinical accuracy progression of decisions. Several studies combined the MRI with other modalities to obtain a fused image which considerably contains more amount of information and much details for diagnosis and reported the effective fusion of MRI with various types of modalities. Image fusion techniques have been widely applied for brain diagnosis and treatment to improve imaging and diagnostic performances such as Positron Emission Tomography (PET)-MRI [9, 10, 11, 12] and Computed Tomography (CT)-MRI [13, 14]. Image fusion are also used to improve prostate cancer detection such as MRI-ultrasound [15], CT-MRI [16, 17] and MRI-transrectal ultrasound [18]. On pelvis gynecological imaging, fusion techniques have been utilized for cancer diagnosis [19, 20]. In ovarian cancer diagnosis, fuzzy-rule-based classifier has been used for fusion [21].

Furthermore, a number of methods have targeted the automatic detection of Lymph Node (LN) including the local-scale-based Hessian analysis method [22] and the learned prior of the spatial distribution [23]. In [24], a graph cut with locally adaptive energy dealt with spatially varying distributions of LN parenchyma and fat caused by in-homogeneous acoustic attenuation. In [25], a segmenting blob-like structure using the graph cut method was adapted and an Ada-Boost classier was trained with features extracted from the segmentation to the 3D chest CT LNs. In [26, 27], the authors used a new method based on integrating segmentation with a learning-based detector. In [28], a cost function was developed to deal with common segmentation problems based on a weighted edge and region homogeneity term. Feuersetein et al. [29] utilized a new approach to automatically detect mediastinal, hilar, and intrapulmonary LN candidates in contrast-enhanced chest CT. Seff et al. [30] used a novel method to automatically detect LNs in CT images, which exploits a hierarchy of classifiers trained on features extracted from 2D views of 3D candidate volumes. Kitasaka et al. [31] used a new method for extracting LN regions from 3D abdominal CT images using a 3D minimal directional difference filter was proposed. In [32], a learned image transformation scheme was explored for producing higher-level inputs of Histograms of Oriented Gradients (HOG) and demonstrated that semantic boundary cues based on HOG descriptors would enrich raw intensity. In [33], a novel approach to segment thoracoabdominal LN clusters combined holistically-nested neural networks and structured optimization. Other works addressed the segmentation of LNs in head and neck CT images [34, 35, 36]. Recently, deep learning techniques have been developed to segment LNs. For instance, Roth et al. [37] generated 2D views via sampling through scale transformation, random translation and rotation to train deep convolutional neural network classifiers. Zhang et al. [38] used a novel deep learning approach, called coarse-to-fine stacked fully convolutional nets to automatically segment LNs in ultrasound images.

However, all these approaches did not exploit DW images where metastatic LNs have a higher intensity than benign ones. In our recent work [39], we used T2-w and DW image fusion step for LN segmentation and classification in cervical cancer MRI. Nevertheless, the segmentation was made by a classic region-growing approach without taking into account the noise and perturbations present in pelvic MRI, PLNs variability as well as the influence of the selection of the initial point.

Additionally, the classification was achieved by a decision tree giving the same degree of reliability to all criteria and the utilized database only contained metastatic PLNs. To address these limitations, we propose in this paper a novel preprocessing-based iterative segmentation approach to correct degradation in the image, iteratively rectify the position of the initial seed point and improve the segmentation results. Furthermore, segmentation step is followed by an automatic classification system based on learning benign and metastatic PLN criteria (morphological and intensity). Moreover, this study aims to detect and stratify PLNs in endometrial and cervical cancer by (1) the combination of several independent preprocessing approaches, (2) the iterative correction of the position of the initial point using region-growing technique to segment PLNs, (3) the registration and fusion of two MR modalities to a common coordinate system using the non-rigid transformation and, (4) the extraction of morphological features of segmented PLNs as well as intensity feature derived from the fused image (previously obtained in (3)) to classify them as suspect or non-suspect. To the best of our knowledge, this is the first work to perform such task. Section 2 presents the proposed method in detail including the MRI and DW image fusion, and the PLN segmentation and classification steps. Finally, section 3 describes the results of our approach, and section 4 concludes the paper.

2. PROPOSED METHOD

In this paper, we firstly propose a semi-automatic computer-aided pelvic approach to extract morphological and intensity features for PLN classification. Specifically, we fuse axial T2-w and DW-MR images. On the other hand, we segment PLNs in axial T2-w images, utilizing a preprocessing-based iterative region-growing method. For PLN segmentation, we label each voxel as PLN or non-PLN thereby generating a 2D binary mask for PLNs. Next, we use the morphological features extracted from the segmented PLNs on T2-w and the intensity feature from the fused image. Ultimately, a decision-based Support Vector Machine (SVM) classification model uses these features to classify candidate PLN as suspect or non-suspect, as illustrated in Fig. 1. In this section, we provide a detailed technical explanation of the proposed method. As shown in Fig. 1, the proposed approach consists of a preprocessing, a fusion and a segmentation and classification stages.

A. Pelvic lymph-node fusion

A typical image fusion technique comprises two steps: (1) image registration and, (2) fusion of features extracted from the registered images. Image registration aligns two images into a common space, where their appearance and structure become similar (Fig. 2). The two imaging modalities used in this paper are axial T2-w and DW images.

1) Axial T2-w image

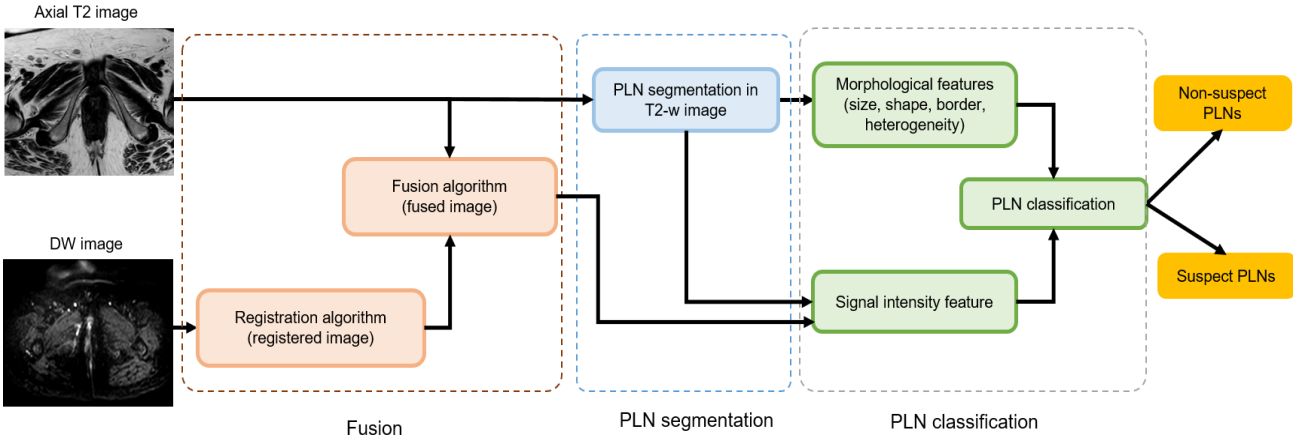

Figure 1. Flowchart of the proposed method. We fuse both axial T2-w and DW imaging modalities. On the other hand, we generate the PLN segmentation mask using T2-w images and preprocessing-based region-growing algorithm. Next, we use the same mask to segment PLNs on fused images. Finally, we extract several features (morphological and intensity) from the segmented PLN to classify them as normal or abnormal.

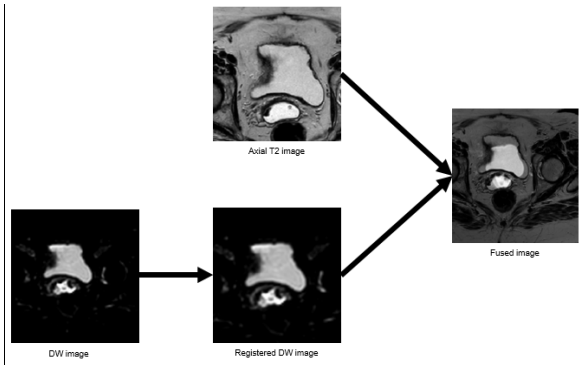

Figure 2. Multimodal MR fusion image. The fused image is obtained by combining information from the DW registered and the T2-w images in order to produce an image that integrates complementary information from both modalities.

T2-w imaging is often used for the evaluation of the PLNs [6], which are clearly differentiated from the hypointense blood vessels and muscles within this sequence (Fig. 3). However, routine MRI is less sensitive and accurate for the detection of PLN metastasis [40]. Thus, the fusion of T2-w and DW-MRI may increase the diagnostic performance.

2) DW image

DW is a promising imaging modality for identifying pelvic gynecological malignancies [41]. DW imaging is based on the movement of water molecules inside voxels giving information about the tissue structure on a microscopic level [41]. The more water molecules diffuse, the lower recorded signal's intensity will be. DW imaging may specify pathologic changes because of the water mobility driven by thermal agitation and the great reliance on its cellular environment. Specifically, tumor tissues are further cellular compared to the native tissues. In case of cancer, anarchic cell proliferation reduces the diffusion of water molecules. Consequently, they show a high signal on the DW-MRI. Because the metastatic PLN intensity is higher than benign PLN one (Fig. 4), the DW sequence is highly useful to detect metastatic PLN. Fused images of both DW-MRI and conventional T2-w image can enhance the detection of metastatic PLNs. Furthermore, early reports involving DW imaging for classifying metastatic PLNs in patients with pelvic gynecological cancer are encouraged. Thus, we propose to fuse both T2-w and DW imaging to improve the

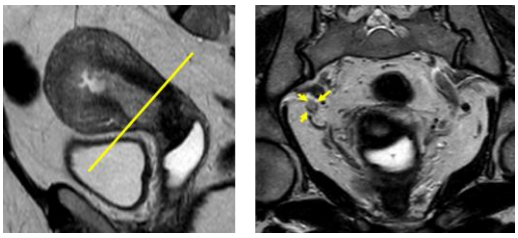

Figure 3. PLN in axial T2-w image. A PLN in a patient with endometrial cancer is visible on axial T2-w image with a hyper signal distinguishing it from the muscles and vessels. PLNs are evaluated on axial slices perpendicular to the cervical axis.

diagnostic accuracy of MRI. To this aim, we first map the DW image space to the axial T2-w image space.

3) Non-rigid registration

Since information is acquired from two images and obtained in the clinical exam, it is usually of complementary nature. The suitable integration of useful details gained from the separate modalities is frequently desired. A first stage in this fusion process is the registration allowing bringing the images involved into spatial alignment. Image registration is popularly used for medical image analysis [42] to align data to a common space. There exist two principal transformation models of registration techniques: (1) affine and rigid transformation, and (2) non-rigid transformation.

Affine and rigid transformation. The rigid transformation is a special case of affine transformation.

Non-rigid transformation. Demon transformation method introduced in [43] is used in this work as it improves rigid trans-formation in registration accuracy [39]. Specifically, Demon registration method is used to register DW and T2-w images and to generate the most comprehensive details provided by both modalities. The axial T2-w image is fixed as a reference and the DW image is automatically moved to the axial T2-w image space. Fig. 5 shows some examples for the automatic alignment the two MR modalities to a common coordinate system. After registration, a fusion step is used to integrate both registered images.

4) Image fusion using wavelet transform

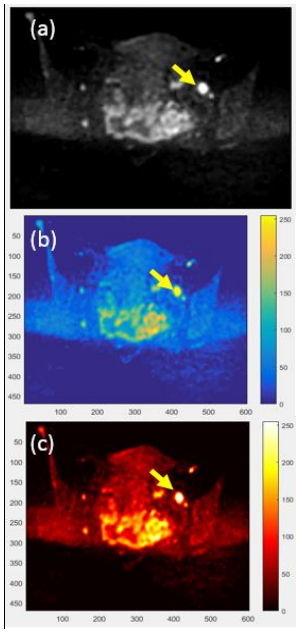

Figure 4. PLN in DW-MR image. (a) DW-MRI with metastatic PLN (yellow arrow). A PLN in a patient with cervical cancer has a bright intensity in DW image. Metastatic PLNs appear with a higher intensity than benign PLNs and it is therefore advantageous to use this sequence for classification. (b) DW image scaled to full range of colors. (c) DW image scaled to full range of hot colors.

Fusion image is an important technique in medical applications [8]. Combining two images into a single one is more suitable for image-processing tasks [44, 45]. The fused image mostly improves the information density and the overall contrast. In this paper, wavelet-based fusion method [46] is used. First, wavelet transform is applied to each image (i.e axial T2-w image and the registered DW image) to decomposed into different multi-frequency bands. Next, at each frequency band, we fuse the corresponding wavelet maps derived from T2-w image with the one derived from the registered DW image. Finally, the fused image is constructed by applying the inverse wavelet transform. An example of our image fusion process is shown in Fig. 2. On the other hand, we locate PLNs and their boundaries in T2-w images using the preprocessing-based iterative region-growing algorithm in order to extract morphological features. Then we segment the fused image to extract the PLN intensity features for ultimate classification.

B. Pelvic lymph-node segmentation

PLN segmentation plays a key role in medical imaging. Segmentation of PLNs in pelvic MR images is a challenging task due to potentially inhomogeneous PLNs density and vicinity structures with similar intensity. A semi-automatic or automatic system that segments PLNs from MR images would therefore be of high clinical use.

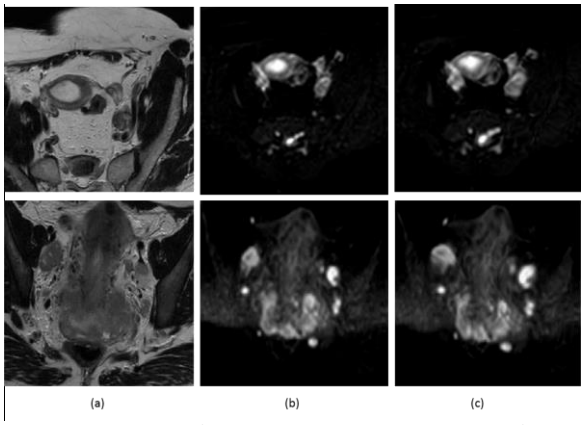

Figure 5. Examples of our registration results. Two types of MRI images (T2-w axial and DW Image) are used. (a) Fixed image is: Axial T2-w image, (b) Moving image is: DW image, and (c) registered image.

Little work has used preprocessing techniques to improve the quality of MRI such as tumor detection in cervical cancer [47] and brain tumor [48].

1) Region-growing segmentation

PLN segmentation has also recognized increasing attention in the last years. PLNs are frequently textured in complex ways; however, they have contiguous regions. Consequently, a region-growing technique for segmentation is chosen. The region-growing method is a pixel-based image segmentation. Particularly, this method iteratively explores the neighboring initial-seed-point pixels and concludes whether the pixel neighbors ought or not to be added to the region. Specifically, regions can be grouped from a manually selected start point. Research has shown that region-growing is based primarily on the selection of the initial point, the characteristics of the image and the homogeneity of the regions. In our work, PLN segmentation by the preprocessing-based iterative region-growing algorithm is initialized with a single point fixed by an expert radiologist. The region-growing approach has been applied for diverse medical image segmentation tasks [49] such as retinal and abdomen liver images [50, 51]. Region-growing segmentation begins with an interactive selection step of the initial seed-point, followed by the region-growing process. Nevertheless, the selection of the initial point is a difficult process and can influence the segmentation results. The proposed iterative region-growing approach (Fig. 7) addresses this limitation by proposing an iterative method to optimize the position of the initial seed-point using the region-growing algorithm.

2) Iterative region-growing segmentation

We firstly propose an iterative region-growing PLN segmentation method to refine the segmentation results of the classic region-growing method. Our iterative

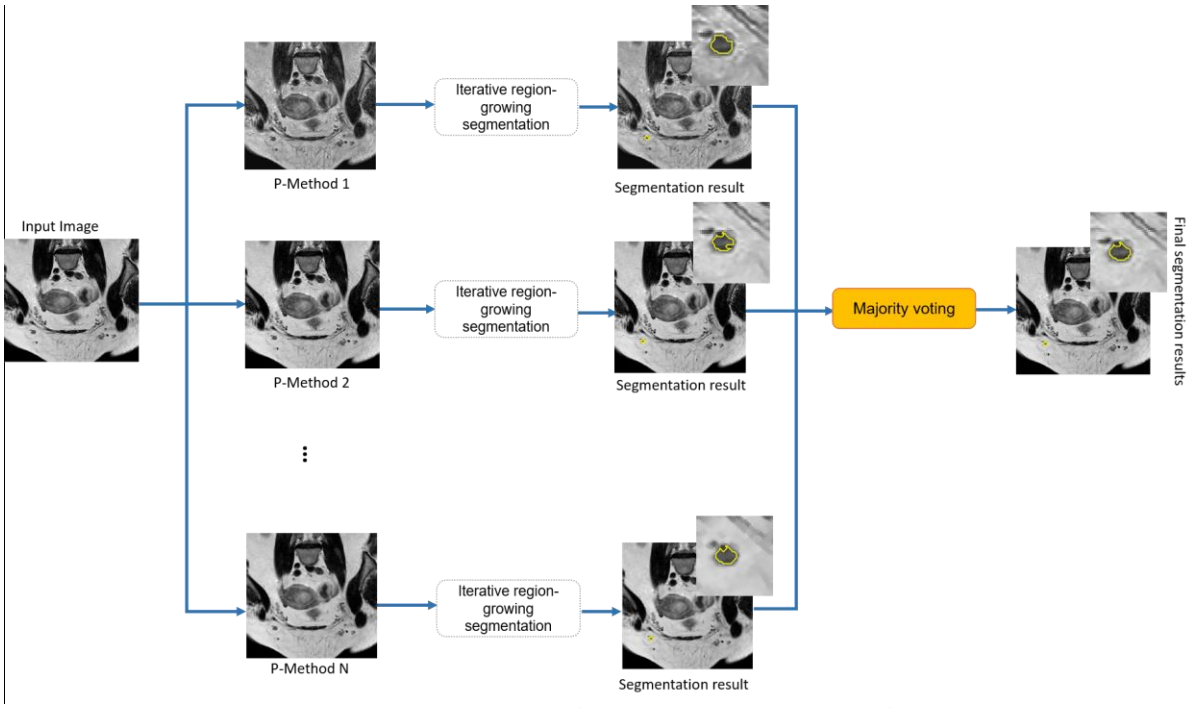

Figure 6. Proposed paralleled preprocessing-based PLN segmentation framework. The proposed approach for PLN segmentation uses an ensemble of preprocessing methods for pelvic cancer segmentation. We first propose N preprocessing techniques. Next, we apply the iterative region-growing approach with the same initial point on images outputted by each of the N preprocessing techniques, respectively. The final segmentation map is obtained by applying the majority voting to segmentation maps, each generated by a preprocessing techniques.

method allows to reduce errors of the semi-automatic PLN segmentation due to a fallible choice of the initial seed-point. The iterative segmentation step is proposed to optimize the initial seed-point selected by the clinician for improving the segmentation results. The principle of the proposed method is presented in (Fig. 7). The first initial seed-points are introduced by a clinician. Then the region-growing algorithm is executed to generate the initial segmentations (K = 1). Based on the center of the $(K-1)^{th}$ segmentation, the region-growing algorithm is repeated the K^{th} time. The algorithm stops when the location of the seed point remains unchanged in two consecutive iterations. On the other hand, image intensity homogeneity is the most used criterion in the growing process. However, pelvic MR images suffer from poor contrast, intensity inhomogeneity, noise and non-uniform lighting. To correct different types of image degradation and to make region-growing approach more adaptive to variations of the dataset, we propose a new approach for endometrial and cervical cancer segmentation based on the iterative region-growing and the different preprocessing techniques (Fig. 6).

3) Region-growing preprocessing-based iterative segmentation

In pelvic MRI, noise is a common issue which restricts image accuracy. Additionally, the metastatic PLN is composed of tumor cells, native PLN tissue and necrosis. Therefore, this problem can be overcome by using different preprocessing techniques. Especially, in this paper, several independent processing approaches for endometrial and cervical cancer MRI are used in order to enhance contrast, improve image quality, suppress noise, reduce perturbations and to address the limitation of depending on a single preprocessing method (Fig. 6). Next, we apply the iterative region-growing approach to the processed images outputted by each specific processing method. Finally, through applying majority voting to our segmentation maps, we obtain the target label map. Our three preprocessing approaches used for pelvic gynecological MRI are detailed below.

Histogram-based MRI preprocessing. Pelvic MR images are exhibited by close contrast values. To reveal more image details, raise overall contrast and redistribute the pixel intensity, we use the Rayleigh distribution (P-Method 1).

Smoothing-and-adjustment based MRI preprocessing. For the second method (P-Method 2), the Gaussian filter is utilized in order to smooth images and remove noise and unwanted details in pelvic MRI. The Gaussian filter is followed by contrast adjustment. The latter is used to increase the contrast of pelvic MRI. Additionally, it remaps image intensity values to the full display range of the data type allowing to sharply differentiate between the PLN and its boundary.

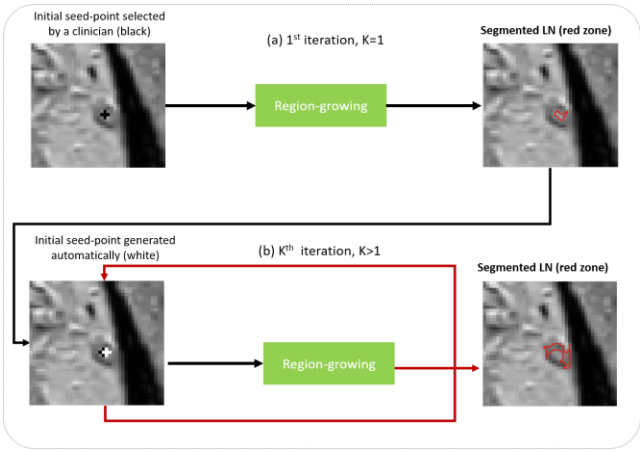

Figure 7. Iterative segmentation method using RG algorithm. (a) Generation of initial LN segmentation (red zone) by RG method based on initial seed-point selected by clinician (black), (b) Iterative improvement loop. Here we use a RG algorithm for LN segmentation, but other semi-automatic methods can be used. The RG algorithm can be applied iteratively until segmentation is satisfactory. For the K^{th} iteration, we use the center of the LN generated at the end of the $(K-1)^{th}$ iteration (white).

Morphological MRI preprocessing. For the third method (P-Method 3), first we apply the Gaussian filter to smooth images, followed by morphological operations to fill in the holes in pelvic MRI, suppress noise, and generate a more homogeneous texture. In particular, we apply their closing and opening successively. Additionally, this approach allows filtering the false positives in the closing and the false negatives in the opening without causing a loss of useful information.

The following section depicts the morphological MRI criteria for suspect and non-suspect PLNs extracted from the segmented PLNs, used for classification, in endometrial and cervical cancer.

C. Pelvic lymph-node classification

In this paper, we use both fusion and segmentation results to improve the PLNs detection performance. Specifically, we combine the anatomical features of the PLN appearance with the intensity feature extracted from the fused image. Then we train a classier using these features to decide if the PLN segmented is suspect or non-suspect.

1) Criteria for normal and abnormal nodes in gynecological pelvic cancer MR imaging

Pelvic lymph node size. The nodal size (short axis >1 cm [4]) is a key criterion used to discriminate benign from metastatic PLNs. If the short axis exceeds 10 mm, PLNs will be considered suspect. In [52], pelvic PLNs

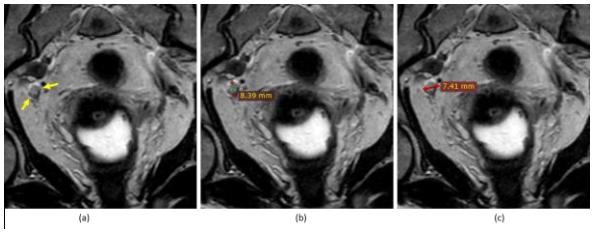

Figure 8. PLN size example. (a) PLN (white arrow), (b) 8.39-mm long axis diameter, (c) 7.41-mm short axis diameter.

with a diameter of ≥ 8 mm were considered suspect. Fig. 8 depicts PLN metastatic with a 8.39-mm long axis diameter, and 7.41-mm short axis diameter, respectively. However, the PLN size alone cannot be used to differentiate benign from metastatic nodes. In fact, the nodal size in axial T2-w cannot distinguish between enlarged inflammatory and metastatic PLNs.

Pelvic lymph node shape. Another morphological feature suggestive of a malignant PLN is the round shape. Specifically, benign PLNs are more likely to be ovoid. On the other hand, they become more circular due to malignant infiltration. Moreover, if the ratio of the long-axis diameter to the short-axis one is less than 2, the PLN is more probable to be malignant [53]. Thus, we use the Ratio as in (1) as a feature.

$$\text{Ratio} = (\text{LongAxis})/(\text{ShortAxis}) \quad (1)$$

However, PLN shape cannot be used as an exclusive criterion for PLN assessment of round parotid and normal submandibular nodes [53].

Pelvic lymph node contour. The PLN contour is a morphological feature that helps to distinguish metastatic PLN from benign one. Specifically, some malignant PLNs are characterized by irregular borders as a result of the extra-capsular disease extension. Metastatic PLNs demonstrate ill-defined borders, while benign PLNs exhibit well-defined borders. Furthermore, the sharp border in the metastatic PLNs is generated by the existing intranodal tumor infiltration that raises the acoustic impedance variance among surrounding and intranodal tissues. Therefore, the PLN border alone cannot be solely relied on to distinguish suspect PLNs from non-suspect ones in a routine clinical practice. Nevertheless, the PLN appearance will be helpful in predicting the node status when utilized with other criteria. We calculate the border values with the energy (E) measure from Gray-Level Co-Occurrence Matrix (GLCM) according to (2).

$$E = \sum_{(i,j)} p(i,j)^2 \quad (2)$$

The energy produces the sum of squared components in the GLCM and produces a value among 0 and 1.

Pelvic lymph node appearance. Normal PLNs are seen as homogeneous structures of intermediate signal intensity on axial T2-w. We define the PLN heterogeneity index (H) using (3).

$$H = -\sum_i P(i)\log[P(i)] \quad (3)$$

where P(i) denotes the histogram of the intensity values of the selected inner region. H is expected to have relatively low values when the region is homogeneous and high values when the histogram values are widely spread, indicating region heterogeneity. The heterogeneity index ranging can have any positive real value.

Pelvic lymph node intensity. Metastatic PLN have an intermediate signal intensity on the axial T2-w MR image. In DW-MRI, metastatic PLNs have high signals. Thus, the use of the intensity of the fused image (axial T2-w and DW image) may improve the classification results. The mean signal intensity (GLCM) for each PLN is calculated and used for classification.

2) Classification

The set of features will be used to classifiy PLN candidate. We have exactly two classes: benign and metastatic PLNs. As a consequence, we choose the SVM classification. The latter is a machine learning technique that has been successfully used for image classification in medical applications [54]. It produces the classification between two groups by finding a decision based on the most informative features of the training set. Specifically, its goal is to find the best hyperplane that separates benign PLNs from metastatic ones.

3. RESULTS AND DISCUSSION

A. Dataset, parameters and evaluation

We carried out the experiments on a pelvic MR database with 48 metastatic PLNs and 59 benign PLNs acquired between January 2016 and December 2017 diagnosed with cervical and endometrial cancer collected from a gynecologic oncology referral center (Maternity Center of Monastir, Fattouma Bourguiba Monastir University Hospital). All patients underwent a regular examination with a 1.5-T MRI system. Axial T2-w 2D turbo spin-echo sequences with voxel size of 0.5×0.5×3 mm were used. All data sets were analyzed by an expert radiologist and PLNs were manually segmented. Malignity and benignity of PLNs were determined by surgical-pathologic examinations. We note that a DW image corresponding to a T2 axial image was provided by an expert. We evaluated our approach on 107 PLNs using SVM classification and leave-one-out cross-validation. The performance of classification results generated by the SVM was assessed with the manual PLN label value (1, -1), (i.e metastatic PLN, benign PLN). The segmentation accuracy was evaluated using the average Dice coefficient (± standard deviation) defined in (4):

$$Dice = 2(A \cap B)/(A + B) \quad (4)$$

where A represents the ground-truth label map delineated by an expert radiologist and B represents the results using the preprocessing-based iterative region-growing approach.

B. Evaluation and comparison methods

In this work, we used iterative region-growing preprocessing-based techniques for PLN segmentation. A thorough demonstration was conducted to determine the interest of iterative region-growing when using the first pre-processing approach. Figure 9 displays our semi-automatic segmentation results as well as the manual segmentation for a selection of five representative PLNs from our database after using the first preprocessing approach (P- Method 1). We determined the Dice coefficient to evaluate the correspondence between

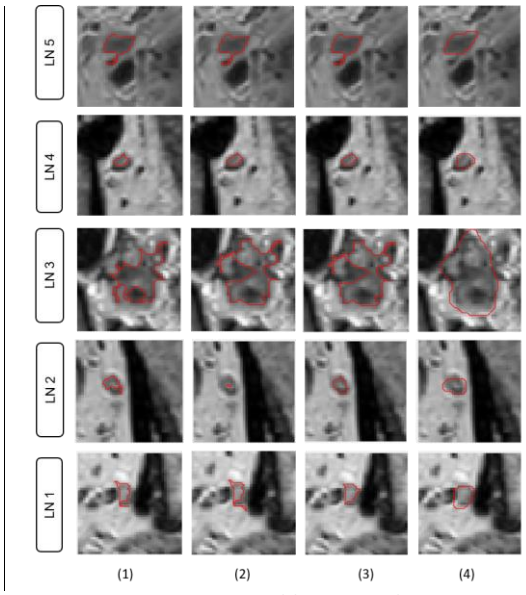

Figure 9. Segmentation results of five PLNs of our database using iterative region-growing technique. Comparison methods: (1) region-growing without initial point optimization (K=1), (2) iterative region-growing with seed point optimization (K=2), (3) iterative region-growing with seed point optimization (K=3), (4) ground-truth: PLN segmented by an expert.

iterative region-growing segmentation and manual segmentation. Our experimental results are reported in Figure 9 and Table 1. We compared the proposed iterative approach of region-growing: (1) region-growing without the optimization of the initial-seed point (K = 1), (2) region-growing with optimization of the initial seed-point (K = 2), and (3) region-growing with two optimizations of the initial seed-point (K = 3). The various experiments showed that the segmentation results remained the same and that the improvement of the precision of the segmentation became negligible starting from K = 3. The proposed method yielded better results ($p < 0.05$) compared to the conventional and iterative region-growing method for K = 2. We observe a significant increase in the average Dice coefficient from 64.68% when using the region-growing method to 66.00% when using the iterative region-growing method (K = 3). Our segmentation method also improved PLN detection and significantly boosted the performance of the conventional region-growing method.

TABLE I. PLN SEGMENTATION RESULTS USING ITERATIVE REGION-GROWING AND HISTOGRAM-BASED PREPROCESSING APPROACH

Method	Mean Dice (%) ± standard deviation
Region-growing (K=1)	64.68% ± 0.2219
Iterative region-growing (K=2)	65.98% ± 0.2140
Iterative region-growing (K=3)	66.00% ± 0.2094

For PLNs 1, 2 and 4 in (Fig. 9), the segmentation results with three iterations were close to the ground-truth. For the segmentation of the PLN3 in Figure 2, we noted the same segmentation result for iterations 2 and 3. In other cases, segmentation remained the same for iterations 1, 2 and 3 (for PLN 5 in Fig. 9).

Fig. 10 reproduces our preprocessing-based iterative region-growing PLN segmentation results along with ground-truth segmentation for a selection of 5 representative PLNs. We determined the Dice coefficient using the manually labeled PLNs to evaluate the correspondence between the preprocessing-based iterative region-growing segmentation and the manual segmentation. Our experimental results are reported in Fig. 10 and Table 2. We compared the proposed region-growing preprocessing-based techniques with: (1) region-growing with-out preprocessing, (2) iterative region-growing without preprocessing, (3) region-growing with histogram-based image preprocessing, (4) iterative region-growing with histogram-based image preprocessing, (5) region-growing with smoothing-and-adjustment based image preprocessing, (6) iterative region-growing with smoothing-and-adjustment based image preprocessing, (7) region-growing with morphological image pre-processing, (8) iterative region-growing with morphological image preprocessing, and (9) region-growing preprocessing-based. The proposed method significantly performed better than all comparison approaches ($p<0.05$) and produced the best segmentation results. The proposed preprocessing-based iterative region-growing PLN segmentation approach achieves the highest average Dice compared to other conventional methods.

We observe a significant increase in the average Dice ratio from 61.37% by region-growing to 66.53% when applying all preprocessing approaches before the paralleled preprocessing-based iterative region-growing algorithm. We note that we use the same initial seed point for all methods. Our segmentation method was also able to improve PLN boundary detection and significantly ($p=0.001$) enhanced the performance when only using region-growing method. The performance can be con-firmed with a larger dataset. In our future work, we will evaluate our method on larger pelvic datasets.

TABLE II. PLN SEGMENTATION RESULTS USING ITERATIVE REGION-GROWING PREPROCESSING-BASED APPROACH

Method	Mean Dice (%) ± standard deviation
(1) Region-growing without preprocessing [39]	61.37 ± 0.2045
(2) Iterative region-growing without preprocessing (K=3)	61.58 ± 0.2078
(3) Region-growing with P-Method 1	64.68 ± 0.2219
(4) Iterative region-growing with P-Method 1 (K=3)	66.00 ± 0.2094
(5) Region-growing with P-Method 2	62.07 ± 0.2566
(6) Iterative region-growing with P-Method 2 (K=3)	62.48 ± 0.2538
(7) Region-growing with P-Method 3	61.95 ± 0.2062
(8) Iterative region-growing with P-Method 3 (K=3)	62.02 ± 0.2044
(9) Region-growing preprocessing-based	64.91 ± 0.2042
(10) Iterative region-growing preprocessing-based (K=3)	66.53 ± 0.1852

Then, we used our segmentation results to classify each PLN as suspect or non-suspect. We note that we did not post-process the PLN boundary outputted by all methods to keep the appearance of PLN since PLNs with lobulated or spiculated contours are more suspect than those with smooth contours [55]. Table 3 recapitulates our PLN classification results. By adding the intensity criterion of the fused image, we produced a better result. The combination of morphological features (size, shape, contour and heterogeneous appearance) and the intensity

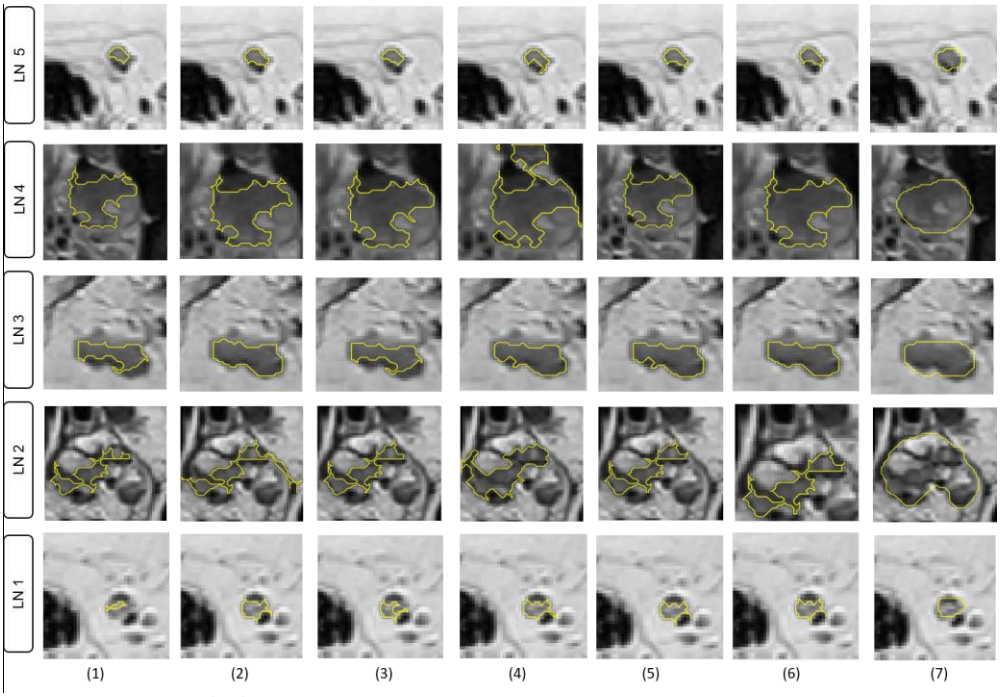

Figure 10: PLN segmentation results for five representative patients using iterative region-growing preprocessing based technique. Comparison methods: (1) region-growing without preprocessing, (2) histogram-based with region-growing, (3) smoothing-based with region-growing, (4) morphological operations with region-growing, (5) all preprocessed with region-growing results aggregated using majority voting, (6) all preprocessed with iterative region-growing results aggregated using majority voting, and (7) ground-truth delineated by an expert radiologist.

(of the merged image) feature extracted from our iterative region-growing preprocessing-based techniques for PLN segmentation boosted the classification accuracy up to 78.50%, in comparison to 71.96% obtained when using morphological features and the intensity of the T2-w image, as well as 76.64% obtained when combining morphological features and the intensity of registered DW image. The proposed approach significantly ($p<0.05$) improved PLNs classification results when only using the morphological features combined with the intensity features derived from (T2-w image/ registered DW image).

TABLE III. PLN CLASSIFICATION RESULTS.

SVM classification using	Accuracy
(Morphological features + intensity feature) (T2-w image)	71.96 %
Morphological features (T2-w image) + intensity feature (registered DW image)	76.64 %
Morphological features (T2-w image) + intensity feature (Fused T2-w & registered DW image)	78.50 %

4. CONCLUSION

PLNs play an important key in the clinical assessment of pelvic cancer. Semi-automatic and automatic PLN classification, as normal or abnormal is highly desired in order to assess the evolution of the disease and treatment planning. In this paper, we proposed a computer-aided pelvic framework using multimodal MR images (axial T2-w and DW) to segment and stratify PLNs as suspect or non-suspect. Our ensemble preprocessing boosting strategy provided three iterative region-growing segmentation results, each leveraging a specific image preprocessing technique to improve the PLN tissue labeling results and optimize the conventional region-growing method. Our framework produced a segmentation accuracy of 66.53% and classification accuracy of 78.50%. In our future work, we will extract more valuable information such as the tumor size from the sagittal T2-w image to enrich our feature set and improve the classification accuracy since PLNs get enlarged with pelvic cancer progression. We will also extend our framework into a fully-automatic approach using advanced methods such as deep learning.

ACKNOWLEDGMENT

This research was carried out in a collaboration with the Department of Gynecology Obstetrics and Radiology of the Maternity Center of Monastir (Fattouma Bourguiba Monastir University Hospital).

REFERENCES

[1] N. Bnouni, I. Rekik, M. S. Rhim, N. Essoukri Ben Amara, Cross-view self-similarity using shared dictionary learning for cervical cancer staging, IEEE Access.

[2] N. Bnouni, I. Rekik, M. S. Rhim, N. Essoukri Ben Amara, Dynamic multi-scale cnn forest learning for automatic cervical cancer segmentation, in: International Workshop on Machine Learning in Medical Imaging, Springer, 2018, pp. 19–27.

[3] N. Singh, S. Arif, Histopathologic parameters of prognosis in cervical cancer–a review, International Journal of Gynecological Cancer 14 (5) (2004) 741–750.

[4] L. Schwartz, J. Bogaerts, R. Ford, L. Shankar, P. Therasse, S. Gwyther, E. Eisenhauer, Evaluation of lymph nodes with recist 1.1, European journal of cancer 45 (2) (2009) 261–267.

[5] C. Köhler, A. Mustea, S. Marnitz, A. Schneider, V. Chiantera, U. Ulrich, J.-P. Scharf, P. Martus, M. A. Vieira, A. Tsunoda, Perioperative morbidity and rate of upstaging after laparoscopic staging for patients with locally advanced cervical cancer: results of a prospective randomized trial, American Journal of Obstetrics & Gynecology 213 (4) (2015) 503–e1.

[6] V. Nicolet, L. Carignan, F. Bourdon, O. Prosmanne, Mr imaging of cervical carcinoma: a practical staging approach, Radiographics 20 (6) (2000) 1539–1549.

[7] J. Chen, Y. Zhang, B. Liang, Z. Yang, The utility of diffusion-weighted mr imaging in cervical cancer, European journal of radiology 74 (3) (2010) e101–e106.

[8] A. P. James, B. V. Dasarathy, Medical image fusion: A survey of the state of the art, Information Fusion 19 (2014) 4–19.

[9] P.-W. Huang, C.-I. Chen, P.-L. Lin, P. Chen, L.-P. Hsu, Pet and mri brain image fusion using wavelet transform with structural information adjustment and spectral information patching, in: Bioelectronics and Bioinformatics (ISBB), 2014 IEEE International Symposium on, IEEE, 2014, pp.1–4.

[10] S. H. M. Alipour, M. Houshyari, A. Mostaar, A novel algorithm for pet and mri fusion based on digital curvelet transform via extracting lesions on both images, Electronic physician 9 (7) (2017) 4872.

[11] P. Rangarajan, Brain tumour detection using discrete wavelet transform based medical image fusion, Biomedical Research 28 (2).

[12] Z. Liu, Y. Song, V. S. Sheng, C. Xu, C. Maere, K. Xue, K. Yang, Mri and pet image fusion using the nonparametric density model and the theory of variable-weight, Computer Methods and Programs in Biomedicine 175 (2019) 73–82.

[13] A. M. Lal, M. Balaji, D. Aju, Multi-level fusion of ct and mri brain images for classifying tumor, International Journal of Enhanced Research in Management & Computer Applications Vol. 3 Issue 8, August 2014.

[14] P. Natarajan, N. Krishnan, N. Soniya, Fusion of mri and ct brain images using histogram equalization, in: Computational Intelligence & Computing Research (ICCIC), 2012 IEEE International Conference on, IEEE, 2012, pp. 1–4.

[15] L. Marks, S. Young, S. Natarajan, Mri–ultrasound fusion for guidance of targeted prostate biopsy, Current opinion in urology 23 (1) (2013) 43.

[16] M. Aoki, A. Yorozu, T. Dokiya, Evaluation of interobserver differences in postimplant dosimetry following prostate brachytherapy and the e cacy of ct/mri fusion imaging, Japanese journal of radiology 27 (9) (2009) 342.

[17] K. L. Maletz, R. D. Ennis, J. Ostenson, A. Pevsner, A. Kagen, I. Wernick, Comparison of ct and mr–ct fusion for prostate post-implant dosimetry, International Journal of Radiation Oncology Biology Physics 82 (5) (2012) 1912–1917.

[18] S. Ahmad, Fusion of mri and trus images for targeted biopsy of prostate, Med Surg Urol 3 (2014) e108.

[19] C.-C. Tsai, C.-S. Tsai, K.-K. Ng, C.-H. Lai, S. Hsueh, P.-F. Kao, T.-C. Chang, J.-H. Hong, T.-C. Yen, The impact of image fusion in resolving discrepant findings between fdg-pet and mri/ct in patients with gynaecological cancers, European journal of nuclear medicine and molecular imaging 30 (12) (2003) 1674–1683.

[20] K. Nakajo, M. Tatsumi, A. Inoue, K. Isohashi, I. Higuchi, H. Kato, M. Imaizumi, T. Enomoto, E. Shimosegawa, T. Kimura, et al., Diagnostic performance of fluorodeoxyglucose positron emission tomography/magnetic resonance imaging fusion images of gynecological malignant tumors: comparison with positron emission tomography/computed tomography, Japanese journal of radiology 28 (2) (2010) 95–100.

[21] A. Assareh, L. G. Volkert, Fuzzy rule base classifier fusion for protein mass spectra based ovarian cancer diagnosis, in: Computational Intelligence in Bioinformatics and Computational Biology, 2009. CIBCB'09. IEEE Symposium on, IEEE, 2009, pp. 193–199.

[22] J. Liu, C.-H. Feng, J. Hua, J. Yao, J. M. White, R. M. Summers, Automatic detection and segmentation of abdominopelvic lymph nodes on computed tomography scans, in: Biomedical Imaging (ISBI), 2012 9th IEEE International Symposium on, IEEE, 2012, pp. 1455–1458.

[23] J. Feulner, S. K. Zhou, M. Hammon, J. Hornegger, D. Comaniciu, Lymph node detection and segmentation in chest ct data using discriminative learning and a spatial prior, Medical image analysis 17 (2) (2013) 254– 270.

[24] J.-w. Kuo, J. Mamou, Y. Wang, E. Saegusa-Beecroft, J. Machi, E. J. Feleppa, Segmentation of 3-d high-frequency ultrasound images of human lymph nodes using graph cut with energy functional adapted to local intensity distribution, IEEE transactions on ultrasonics, ferroelectrics, and frequency control 64 (10) (2017) 1514–1525.

[25] J. Feulner, S. K. Zhou, M. Hammon, J. Hornegger, D. Comaniciu, Segmentation based features for lymph node detection from 3-d chest ct, in: International Workshop on Machine Learning in Medical Imaging, Springer, 2011, pp. 91–99.

[26] A. Barbu, M. Suehling, X. Xu, D. Liu, S. K. Zhou, D. Comaniciu, Automatic detection and segmentation of axillary lymph nodes, in: International Conference on Medical Image Computing and Computer-Assisted Intervention, Springer, 2010, pp. 28–36.

[27] A. Barbu, M. Suehling, X. Xu, D. Liu, S. K. Zhou, D. Comaniciu, Automatic detection and segmentation of lymph nodes from ct data, IEEE Transactions on Medical Imaging 31 (2) (2012) 240–250.

[28] R. R. Beichel, Y. Wang, Computer-aided lymph node segmentation in volumetric ct data, Medical physics 39 (9) (2012) 5419–5428.

[29] M. Feuerstein, D. Deguchi, T. Kitasaka, S. Iwano, K. Imaizumi, Hasegawa, Y. Suenaga, K. Mori, Automatic mediastinal lymph node detection in chest ct, in: Medical Imaging 2009: Computer-Aided Diagnosis, Vol. 7260, International Society for Optics and Photonics, 2009, p. 72600V.

[30] A. Se , L. Lu, K. M. Cherry, H. R. Roth, J. Liu, S. Wang, J. Ho man, B. Turkbey, R. M. Summers, 2d view aggregation for lymph node detection using a shallow hierarchy of linear classifiers, in: International Conference on Medical Image Computing and Computer-Assisted Intervention, Springer, 2014, pp. 544–552.

[31] T. Kitasaka, Y. Tsujimura, Y. Nakamura, K. Mori, Y. Suenaga, M. Ito, S. Nawano, Automated extraction of lymph nodes from 3-d abdominal ct images using 3-d minimum directional difference filter, in: International Conference on Medical Image Computing and Computer-Assisted Intervention, Springer, 2007, pp. 336–343.

[32] A. Se , L. Lu, A. Barbu, H. Roth, H.-C. Shin, R. M. Summers, Leveraging mid-level semantic boundary cues for automated lymph node detection, in: International Conference on Medical Image Computing and Computer-Assisted Intervention, Springer, 2015, pp. 53–61.

[33] I. Nogues, L. Lu, X. Wang, H. Roth, G. Bertasius, N. Lay, J. Shi, Y. Tsehay, R. M. Summers, Automatic lymph node cluster segmentation using holistically-nested neural networks and structured optimization in ct images, in: International Conference on Medical Image Computing and Computer-Assisted Intervention, Springer, 2016, pp. 388–397.

[34] L. J. Stapleford, J. D. Lawson, C. Perkins, S. Edelman, L. Davis, M. W. McDonald, A. Waller, E. Schreibmann, T. Fox, Evaluation of automatic atlas-based lymph node segmentation for head-and-neck cancer, International Journal of Radiation Oncology Biology Physics 77 (3) (2010) 959– 966.

[35] A. Chen, M. A. Deeley, K. J. Niermann, L. Moretti, B. M. Dawant, Combining registration and active shape models for the automatic segmentation of the lymph node regions in head and neck ct images, Medical physics 37 (12) (2010) 6338–6346.

[36] J. Dornheim, H. Seim, B. Preim, I. Hertel, G. Strauss, Segmentation of neck lymph nodes in ct datasets with stable 3d mass-spring models: Segmentation of neck lymph nodes, Academic Radiology 14 (11) (2007) 1389–1399.

[37] H. R. Roth, L. Lu, J. Liu, J. Yao, A. Se , K. Cherry, L. Kim, R. M. Summers, Improving computer-aided detection using convolutional neural networks and random view aggregation, IEEE transactions on medical imaging 35 (5) (2016) 1170–1181.

[38] Y. Zhang, M. T. Ying, L. Yang, A. T. Ahuja, D. Z. Chen, Coarse-to-fine stacked fully convolutional nets for lymph node segmentation in ultrasound images, in: Bioinformatics and Biomedicine (BIBM), 2016 IEEE International Conference on, IEEE, 2016, pp. 443–448.

[39] N. Bnouni, O. Mechi, I. Rekik, M. S. Rhim, N. Essoukri Ben Amara, Semi-automatic lymph node segmentation and classification using cervical cancer mr imaging, in: 2018 4th International Conference on Advanced Technologies for Signal and Image Processing (ATSIP), IEEE, 2018, pp. 1–6.

[40] K. Lv, H.-m. Guo, Y.-j. Lu, Z.-x. Wu, K. Zhang, J.-k. Han, Role of 18f-fdg pet/ct in detecting pelvic lymph-node metastases in patients with early-stage uterine cervical cancer: comparison with mri findings, Nuclear medicine communications 35 (12) (2014) 1204–1211.

[41] S. Dhanda, M. Thakur, R. Kerkar, P. Jagmohan, Diffusion-weighted imaging of gynecologic tumors: diagnostic pearls and potential pitfalls, Radiographics 34 (5) (2014) 1393–1416.

[42] A. A. Goshtasby, 2-D and 3-D image registration: for medical, remote sensing, and industrial applications, John Wiley & Sons, 2005.

[43] J.-P. Thirion, Image matching as a diffusion process: an analogy with maxwell's demons, Medical image analysis 2 (3) (1998) 243–260.

[44] G. Pajares, J. M. De La Cruz, A wavelet-based image fusion tutorial, Pattern recognition 37 (9) (2004) 1855–1872.

[45] X. Yuan, X. Yuan, Fusion of multi-planar images for improved three-dimensional object reconstruction, Computerized Medical Imaging and Graphics 35 (5) (2011) 373–382.

[46] H. Li, B. Manjunath, S. K. Mitra, Multisensor image fusion using the wavelet transform, Graphical models and image processing 57 (3) (1995) 235–245.

[47] N. Bnouni, H. Ben Amor, I. Rekik, M. S. Rhim, B. Solaiman, N. Essoukri Ben Amara, Boosting cnn learning by ensemble image preprocessing methods for cervical cancer mr image segmentation, in: International conference on Sensors, Systems, Signals and advanced technologies (SSS), 2018.

[48] K. Kamnitsas, W. Bai, E. Ferrante, S. McDonagh, M. Sinclair, N. Pawlowski, M. Rajchl, M. Lee, B. Kainz, D. Rueckert, et al., Ensembles of multiple models and architectures for robust brain tumour segmentation, arXiv preprint arXiv:1711.01468.

[49] X. Zhang, X. Li, Y. Feng, A medical image segmentation algorithm based on bi-directional region growing, Optik-International Journal for Light and Electron Optics 126 (20) (2015) 2398–2404.

[50] H. Jiang, B. He, D. Fang, Z. Ma, B. Yang, L. Zhang, A region growing vessel segmentation algorithm based on spectrum information, Computational and mathematical methods in medicine 2013.

[51] Y. Q. Zhao, X. H. Wang, X. F. Wang, F. Y. Shih, Retinal vessels segmentation based on level set and region growing, Pattern Recognition 47 (7) (2014) 2437–2446.

[52] A. Heuck, J. Scheidler, R. Kimmig, U. Mueller-Lisse, M. Steinborn, T. Helmberger, M. Reiser, Lymph node staging in cervix carcinomas: the results of high-resolution magnetic resonance tomography (mrt) with a phased-array body coil, RoFo: Fortschritte auf dem Gebiete der Rontgenstrahlen und der Nuklearmedizin 166 (3) (1997) 210–214.

[53] H. Steinkamp, M. Cornehl, N. Hosten, W. Pegios, T. Vogl, R. Felix, Cervical lymphadenopathy: ratio of long-to short-axis diameter as a predictor of malignancy, The British journal of radiology 68 (807) (1995) 266–270.

[54] C.-S. Lo, C.-M. Wang, Support vector machine for breast mr image classification, Computers & Mathematics with Applications 64 (5) (2012) 1153–1162.

[55] H. J. Choi, S. H. Kim, S.-S. Seo, S. Kang, S. Lee, J.-Y. Kim, Y. H. Kim, J. S. Lee, H. H. Chung, J.-H. Lee, et al., Mri for pretreatment lymph node staging in uterine cervical cancer, American Journal of Roentgenology 187 (5) (2006) W538–W543.

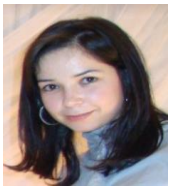

NESRINE BNOUNI received the degree in computer engineering and the master's degree in intelligent and communicating system from the National Engineering School of Sousse, where he is currently pursuing the Ph.D. degree with the Electrical Department. She is currently a Member of the Laboratory of Advanced Technology and Intelligent Systems, National Engineering School of Sousse, and also a Member of the Brain And SIgnal Research and Analysis Laboratory, Istanbul Technical University. She is carrying out research in computer vision and image processing focused on cervical cancer diagnosis and treatment using magnetic resonance imaging.

ISLEM REKIK received the Ph.D. degree in neuroimaging and computer sciences from The University of Edinburgh, in 2014. She was a Postdoctoral Research Scholar with the IDEA Lab, University of North Carolina, She is currently an Assistant Professor (Lecturer) with Istanbul Technical University and an Honorary Researcher with the School of Science and Engineering, University of Dundee. She is also the Director of the Brain And SIgnal Research & Analysis Laboratory. She is a Program Committee Member of leading international medical image analysis conferences and workshops, including MICCAI, IPMI, *Machine Learning in Medical Imaging*, *Connectomics in NeuroImaging* (CNI), and *Deep Learning in Medical Imaging* and an Area Chair of MICCAI 2019 and Medical Imaging with Deep Learning 2019 Conference. She has co-organized Predictive Intelligence in MEdicine and CNI workshops, in conjunction with MICCAI 2018. Her research works aim to infuse advanced computer vision and machine-learning methods into big neuroimaging, and signal data analysis for improving healthcare and wellbeing.

MOHAMED SALAH RHIM was with the hospital center of Blois in France. He is currently an Assistant Professor in gynecology-obstetrics with the Faculty of Medicine of Monastir. His research interest includes cervical cancer imaging.

NAJOUA ESSOUKRI BEN AMARA was the Director of ENISo, University of Sousse, Tunisia, from 2008 to 2011. Since 2011, she has been the President of the Tunisian Association of Innovative Techniques of Sousse. She is currently a Full Professor of electrical engineering with the National School of Engineers of Sousse, ENISo. She is a Founding Member and the Director of the research laboratory LATIS-Laboratory of Advanced Technology and Intelligent Systems. She was a Coordinator of several European projects (Euromed 3C3 and Tempus). She initiated multiple collaborations with international research laboratories and socio-economic organizations. Her research interests include pattern recognition, document analysis, multimodal biometric, medical image processing, computer vision, with application to the segmentation of documents, biometric recognition, individuals, and detection/monitoring multi-object. She has a wide national and international visibility, as she chaired several national committees and chaired/co-chaired various international scientific conferences. She acts in many program committees and belongs to several scientific ones.